Early differentiation of the bulk silicate Earth as recorded by the oldest mantle reservoir

Xuan-Ce Wang[1*] Zheng-Xiang Li[1]Xian-Hua Li[2]

1. *ARC Centre of Excellence for Core to Crust Fluid Systems (CCFS), The Institute for Geoscience Research (TIGeR), Department of Applied Geology, Curtin University, GPO Box U1987, Perth, WA 6845, Australia*
2. *State Key Laboratory of Lithospheric Evolution, Institute of Geology and Geophysics, Chinese Academy of Sciences, P.O. Box 9825, Beijing 100029, China*

* Corresponding author. Department of Applied Geology, Curtin University, GPO Box U1987, Perth, WA 6845, Australia.
Phone: +61 8 9266 2453
Fax: +61 8 9266 3153
*E-mail: X.Wang3@curtin.edu.au

ABSTRACT

An emerging challenge for understanding the Earth system is to determine the relative roles of early planetary processes versus progressive differentiation in shaping the Earth's chemical architecture. An enduring tenet of modern chemical geodynamics is that the Earth started as a well-mixed and homogeneous body which evolved progressively over the geologic time to several chemically distinct domains. As a consequence, the observable chemical heterogeneity in mantle-derived rocks has generally been attributed to the Earth's dynamic evolution over the past 4.5 Ga. However, the identification of chemical heterogeneity formed during the period 4.53–4.45 Ga in the ca. 60 Ma Baffin Bay high-magnesium lavas provides strong evidence that chemical effects of early differentiation can persist in mantle reservoirs to the present day. Here, we demonstrate that such an ancient mantle reservoir is likely composed of enriched and depleted dense melts, and propose a model for early global differentiation of the bulk silicate Earth that would produce two types of dense melts with distinctive chemical compositions in the deep Earth. These dense melts ultimately became parts of the thermo-chemical piles near the core-mantle boundary that have been protected from complete entrainment by subsequent mantle convection currents. We argue that although such dense melts likely exhibit some 'primordial' geochemical signatures, they are not reprehensive of the bulk silicate Earth. Our work provides a strong case for the mantle chemical heterogeneity being formed by a major differentiation event shortly after planet accretion rather than through the subsequent geodynamic evolution.

INTRODUCTION

The Earth's mantle is chemically heterogeneous at all scales (Hofmann, 1997; Zindler and Hart, 1986). Knowledge about the chemical composition and differentiation of the primordial silicate Earth is crucial for understanding how the Earth's mantle works (e.g., Caro, 2011; Hofmann, 1997; Zindler and Hart, 1986). However, chemical signatures related to the Earth's early differentiation are believed to have largely been scrambled or diluted by whole mantle convection, tectonic-plate recycling and continuous exchanges between the mantle and crust over the past 4.5 Ga (e.g., Allègre, 1982; Caro, 2011). As a result, the isotopic and chemical heterogeneities observed in modern mantle-derived rocks are generally believed to reflect later production and recycling of oceanic and continental crust through geological time, and thus bear no direct signature of the primordial silicate Earth (e.g., Allègre, 1982; Hofmann, 1997; Zindler and Hart, 1986). This led to the widely held believe that the Earth started as a well-mixed homogeneous body that evolved progressively over geologic time to several chemically distinct domains (Allègre, 1982; Hofmann, 1997; Zindler and Hart, 1986). However, we demonstrated here that the very-early-formed chemical heterogeneity as recorded by the oldest mantle reservoir can persist in mantle reservoirs to the present day.

The ca. 60 Ma old Baffin Bay picrites between Baffin Island and West Greenland (BIWG) are among the earliest manifestations of the ancestral Iceland mantle plume. The high $^{3}He/^{4}He$ end-member of the mantle composition range (up

to 50 R_A, where R_A is the atmospheric value of 1.39×10^{-6}) (Starkey et al., 2009) in the picrites may signify an undegassed primitive mantle source or isolated primordial He-rich reservoir that is a residue of ancient mantle depletion (Heber et al., 2007). The recent landmark discovery of a primitive Pb isotopic composition confirmed that the BIWG lavas were derived from a deep-Earth reservoir preserved at the core-mantle boundary (CMB) that has remained isolated since the earliest days of planetary accretion some 4.5 Ga (Jackson et al., 2010). Jackson et al. (2010) proposed that the composition of such an ancient reservoir is representative of the bulk silicate Earth (BSE) (Andreasen et al., 2008) 'parental to all mantle reservoirs'.

DISCUSSION

A previous back-calculation based on the two highest $^3He/^4He$ samples (DUR8 and BI/PI/25) (Jackson et al., 2010) suggested that the oldest mantle reservoir represents a residue of an ancient global depletion event. If this is true, the estimated Nb/La ratio for the oldest mantle reservoir should be similar to typical depleted mantle reservoirs. However, such a back-calculation resulted in an extremely high Nb/La ratio of 1.41 that is much higher than any known depleted reservoir, such as modern depleted mid-ocean-ridge basalt (MORB) mantle reservoirs (Nb/La = 0.64–0.97; Workman and Hart, 2005) and early depleted reservoirs (Nb/La = 0.74–0.79; Carlson and Boyet, 2008). Furthermore, uncontaminated BIWG picrites (Starkey et al., 2009) and their olivine-hosted melt inclusions (Starkey et al., 2012) exhibit a large range of isotopic and chemical compositions, overlapping that of both typical depleted

and enriched mantle reservoirs. There has been no evidence suggesting the existence of either depleted melt inclusions in the enriched picrites, or enriched inclusions in the depleted picrites (Starkey et al., 2012), arguing strongly against the derivation of the picrites from a single depleted reservoir. This emphasizes the needs for a better understanding of the nature and origin of the oldest mantle reservoirs, and the chemical heterogeneity of the BIWG picrites holds the key for unrevealing early global differentiation of the BSE (e.g., Bennett et al., 2007; Caro, 2011; Lee et al., 2010; Nomura et al., 2011). Before discussing the characteristics of the BIWG source, we first use a set of criteria (Figs. 1–2) to first strip-off the highly evolved BIWG samples, and then reconstruct the primary melt compositions (Appendix Table S1). The uncontaminated BIWG picrites show a fairly narrow $^{206}Pb/^{204}Pb$ range that plots within the geochrons of 4.53 to 4.40 Ga, whereas the contaminated lavas show a larger $^{206}Pb/^{204}Pb$ range plotting outside this geochron band (Fig. 2h). This confirms the effectiveness of the criteria used for striping-off the effects of assimilation-fractional crystallization. The estimated primary melt compositions and melting pressures suggest melt fractions of ~7 to 22%, that correlate with Sm/Nd, Nb/La, Zr/Sm, Zr/Nb and La/Sm ratios (Fig. 3). Thus, refractory lithophile element ratios of the less-evolved BIWG picrites and partial melting conditions can be used to examine the nature and origin of such an ancient mantle reservoir.

The refractory lithophile element ratios and isotopic results of the less-evolved BIWG picrites suggest that their source likely contains two extreme end-member components (Fig. 4 and Appendix Fig. R2). This is consistent with the end-members

defined by olivine-hosted melt inclusions from uncontaminated BWG picrites (Fig. 4a–c). The compositions of the two end-member sources were estimated based on forward partial melting modelling (Fig. 4). Melt fractions for the enriched and depleted end-member melts are constrained by the correlation of refractory lithophile element ratios with melt fractions (Fig. 3). The best estimate for the enriched end-member source is Sm/Nd = 0.33 (corresponding to $^{147}Sm/^{144}Nd = 0.1977$), La/Sm = 1.7, Nb/La = 1.4, Zr/Sm = 29.2, Zr/Nb = 12.2, and εNd_{60} = +2 to +4. The estimated depleted end-member source, on the other hand, has Sm/Nd = 0.38 ($^{147}Sm/^{144}Nd$ = 0.217), La/Sm = 0.77, Nb/La = 0.62, Zr/Sm = 22.1, Zr/Nb = 50.0, and εNd_{60} = +8 to +11. The corresponding parent/daughter ratios of Rb-Sr, Lu-Hf and Re-Os for the two end-member sources are shown in Fig. 4f–h. Because the BIWG source likely formed at 4.5 Ga (Jackson et al., 2010), the above two end-members therefore likely bear important information regarding early global differentiation of the BSE (e.g., Caro, 2011).

The depleted end-member source likely represents a residual of the global depletion event early in the Earth's history (Jackson et al., 2010). This end-member source is highly depleted relative to chondritic BSE, with refractory lithophile element ratios similar to that of modern depleted MORB mantle and early depleted reservoirs, and Nd-Sr-Hf isotope comparable to early depleted reservoirs (Fig. 4). The differentiation of the early silicate Earth was expected to produce such an early depleted reservoir with super-chondritic Sm/Nd and Lu/Hf, and sub-chondritic Rb/Sr ratios (Caro and Bourdon, 2010 and references therein), which is similar to that

observed in the depleted end-member source (Figs. 4d–f). Evidence for the existence of such an early depleted reservoir is mainly from superchondritic $^{142}Nd/^{144}Nd$ ratios (e.g., Caro, 2011) and coupled ^{182}W–^{142}Nd anomalies (Moynier et al., 2010) in most terrestrial samples.

However, it has been unclear whether a complementary early-formed enriched component exists in modern silicate domains and, if any, how it affects modern mantle reservoirs (e.g., Andreasen et al., 2008; Caro, 2011). The enriched end-member source calculated here is characterized by a higher superchondritic Nb/La ratio (1.4) and broadly chondritic Sm/Nd, La/Sm and Zr/Nb ratios and Nd isotopes (Fig. 4b–d). The following argument suggests that the decoupling of Nb/La ratios from Sm/Nd ratios and associated Nd isotopes is a lower mantle signature. Bulk solid-melt Sm/Nd partition coefficients ($^{bulk}D_{Sm/Nd}$) at upper mantle pressures are about 2, and decrease to unity at lower mantle pressures (Appendix Table S3 and Fig. R3). Furthermore, experimental partition coefficients for lower mantle minerals show that rare earth elements are strongly compatible in Ca-perovskite (Corgne et al., 2005). By contrast, Nb, Ta, Pb, Rb and Ba are incompatible in Ca-perovskite. As a consequence, melt segregated from a basal magma ocean (Nomura et al., 2011) will be depleted in rare earth elements, U and Th, but enriched in Rb, Ba, and Nb, Ta, and Sr (Jackson et al., 2010) (Fig. 5a). Therefore, freezing of a magma ocean with a nonchondritic BSE composition (Sm/Nd = 0.343, Nb/La = 0.89; Fig. 5a) initiated at the base of mantle (Caro et al., 2005 and references therein) would have resulted in an incompatible element-enriched residual melt with Nb/La, Zr/Nb, La/Sm, Zr/Sm and

Sm/Nd ratios and Nd-Sr-Os isotopes, as observed in the BIWG enriched end-member (Figs. 4 and 5a). In contrast, differentiation of a chondritic BSE (McDonough and Sun, 1995) cannot produce the enriched end-member source (Fig. 2d and f). Together with the homogeneous super-chondritic $^{142}Nd/^{144}Nd$ ratios in the BIWG picrites (de Leeuw et al., 2010), we propose that the enriched end-member source originated from a nonchondritic BSE in the lower mantle.

Because both the depleted and enriched BIWG end-member sources possess primordial (high) $^{3}He/^{4}He$ signatures (Starkey et al., 2012), the above two end-member sources were most likely generated in an undegassed deep Earth. It has been argued that differentiation of early silicate Earth in deep Earth can generate undegassed dense melts concentrating at the CMB (e.g., Lee et al., 2010; Nomura et al., 2011) and ultimately result in the primordial time-integrated high $^{3}He/^{4}He$ of ca. 60 R_A at 60 Ma (Lee et al., 2010) (Fig. 5b). The large range in the estimated Th, U and He contents implies that the oldest mantle reservoir should evolve to have $^{3}He/^{4}He$ = 33–54 R_A after ca. 4.4 Ga of isolation from whole-mantle convection (Fig. 5b). This coincides well with observed values in the uncontaminated BIGW picrites (Fig. 3B). Although the early-formed dense melts exhibit some 'primordial' isotopic signatures, providing an elegant argument for the survival of a primitive geochemical component in the mantle, we argue that they did not preserve the true primordial bulk silicate Earth composition in terms of major element and key trace element compositions.

177 **CONCLUSION**

178 Understanding the way of early silicate Earth differentiation requires knowledge of
179 the density contrast between solid and melt fractions (e.g., Lee et al., 2010; Nomura et
180 al., 2011). Positive and negative melt buoyancies yield drastically different
181 geodynamical models. The prevailing view of differentiation of Earth's silicate
182 mantle is driven by extraction of low-density melts. As the mantle upwells and
183 decompresses across its solidus, it partially melts. These low-density melts rise to the
184 surface and form the continental and oceanic crusts, driving the differentiation of the
185 silicate part of the Earth. Lee et al. (2010) proposed a fresh perspective on the way of
186 early Earth silicate Earth differentiation if liquids sink instead of rise. Under certain
187 high-pressure conditions in upper mantle, it has been suggested that peridotite partial
188 melts may be more dense than solid peridotite because such liquids are Fe-rich and
189 more compressible than solids (e.g., Lee et al., 2010; Miller et al., 1991; Stolper et al.,
190 1981; Suzuki et al., 1998). Recent experimental determined iron partitioning over the
191 entire mantle pressure range suggested that liquid formed at ≥1,800 km becomes
192 denser than coexisting solid in the lower mantle (Nomura et al., 2011). It should be
193 pointed out that the behaviour of solid–liquid iron partitioning in Earth's deep mantle
194 is still poor constrained and highly debated (e.g., Andrault et al., 2012).

195 We use Figure 6 to illustrate how global differentiation of the early silicate Earth
196 during 4.55–4.40 Ga may have produced two types (depleted and enriched) of dense
197 melts in an undegassed deep Earth. If crystallization of a magma ocean began at the

198 base of the Earth's mantle and progressed upward (Caro et al., 2005 and references
199 therein), the global differentiation of the BSE would have occurred in two
200 independent layers at >1,800 km and ≤1,800 km depths (Nomura et al., 2011) (Fig.
201 6a). With progressive crystallization, the density contrast (Nomura et al., 2011) would
202 produce an enriched denser liquid phase at the core-mantle boundary, enriching in
203 incompatible trace elements (Rb, Ba, Nb, Pb, and Sr) including volatile species
204 (Labrosse et al., 2007). In contrast, within the upper layer (≤1,800 km), as the
205 crystallization proceeded, the residual liquid would rise buoyantly until a small
206 fraction (≤1%) of melt ultimately formed a protocrust at the Earth surface, resulting in
207 depleting 60% of the silicate Earth. This is consistent with the 60% depletion
208 constraint by the Nd budget of the crust (Caro et al., 2005 and references therein). The
209 depleted dense melt may have been generated by high degree partial melting of
210 peridotite at about 300-410 km depths (Lee et al., 2010) shortly after magma ocean
211 crystallization (Fig. 6a). The above two types of dense melts would result in materials
212 constituting the present-day thermo-chemical piles hosted within the two large
213 low-shear-wave-velocity provinces above the CMB (e.g., Jackson and Carlson, 2011;
214 Nomura et al., 2011), that have been protected from complete entrainment by
215 subsequent mantle convection currents (e.g., Caro, 2011; Nomura et al., 2011).

216 Because the homogeneous superchondritic $^{142}Nd/^{144}Nd$ signatures in the BIWG
217 picrites (de Leeuw et al., 2010) were mainly formed within the Earth's first 30 Ma
218 (Caro et al., 2008), both the enriched and the depleted end-members likely formed at
219 4.53–4.45 Ga, as independently constrained by the primitive Pb isotopes (Fig. 1h).

This coincides with a mean early mantle differentiation age of 4.51 ± 0.02 Ga (Bennett et al., 2007). The identification of such very-early-formed chemical heterogeneity in modern mantle-derived rocks therefore provides strong evidence that the BSE was affected by non-uniformitarian processes early on in Earth history, resulting in extremely local chemical differentiation (e.g., Bennett et al., 2007). Furthermore, such chemical effects can persist in mantle reservoirs to the present day, which is attributed to a combination of compositionally induced high density and low viscosity (e.g., Caro, 2011; Nomura et al., 2011). This provides a strong case against the popular chemical geodynamic model that the observable isotopic and elemental heterogeneity in mantle-derived rocks mainly reflects the presence of several end-member mantle reservoirs formed through the Earth's younger geodynamic processes (e.g., Hofmann, 1997; Zindler and Hart, 1986). Thus, an emerging challenge for the understanding the Earth system is to determine the relative roles of early planetary processes versus progressive differentiation in shaping the Earth's chemical architecture.

How such a dense chemical layer can be sampled and brought to the surface is an important question. Geological evidence related to supercontinent reconstructions (e.g., Li and Zhong, 2009) shows that both the location and formation of superplumes were dominantly controlled by the first order geometry of global subduction zones. Recent studies proposed that sinking subducted slabs could not only push the dense chemical layer upward, but also push the thermal boundary layer to form thermal-chemical domes (Steinberger and Torsvik, 2012), enhancing or triggering

thermal instability (Fig. 6b). The physical properties of mantle plumes also imply that materials from the dense chemical layer near the CMB should only be a minor component of mantle plumes and thus can only be identified in the earliest phase of high temperature melts (picrites and komatiites) (e.g., Campbell and O'Neill, 2012).

Acknowledgements

We thank S.A. Wilde (Curtin University) for constructive suggestions and proof-reading. This work was supported by the National Science Foundation of China (grants 41173038, 40803010 and 40973044) and the Australian Research Council (ARC) Discovery Project grant (DP110104799). This is TIGeR publication No. xx and contribution xx from the ARC Centre of Excellence for Core to Crust Fluid Systems (http://www.ccfs.mq.edu.au/).

254 Figure Caption

255 Fig. 1. Variation of selected oxides, trace element ratios, and isotopes as a function of
256 MgO concentration in the BIWG lavas (Dale et al., 2009; Jackson et al., 2010; Larsen
257 and Pedersen, 2009; Lightfoot et al., 1997; Robillard et al., 1992; Schaefer et al., 2000;
258 Starkey et al., 2009). Black dashed lines in (**a-f**) represent the BIWG lavas evolution
259 path. The solid black lines with arrows indicate the effect of fractional crystallization
260 of single minerals on magmatic evolution (Wang et al., 2012). These figures show
261 that after stripping-off the effect of crustal contamination, the samples with MgO>12
262 wt.% are only affected by olivine fractional crystallization or accumulation. Due to
263 the extremely high incompatibility in olivine, the incompatible trace element ratios of
264 the samples with MgO >12 wt.% reflect the contribution of source region and/or
265 crustal contamination.

266 Fig. 2. Evaluating the effects of crustal contamination on BIWG magma compositions.
267 This figure shows that the effects of assimilation-fractional crystallization (AFC) on
268 the samples with SiO_2 ≤50 wt.%, MgO >12 wt.%, and εNd(t)>+2 are insignificant if
269 any. Black curves indicate evolution of $^{207}Pb/^{204}Pb$ versus $^{206}Pb/^{204}Pb$ starting from
270 the initial Pb-isotope composition of Canyon Diablo (Paul et al., 2002). Also shown
271 are 4.568 Ga, 4.53 Ga, and 4.45 Ga geochrons (Jackson et al., 2010). Pb* =
272 $2Pb_N/(Ce_N + Pr_N)$, subscript N indicates the CI-chondrite (McDonough and Sun, 1995)
273 normalized values.

Fig. 3. Plots of incompatible trace element ratios versus calculated melt fraction number (**F, %**). The melt fraction number is calculated by function A1 and A2 in the appendix of Putirka et al. (2007). The calculated melt fraction broadly correlates with the incompatible trace element ratios from the uncontaminated picrites. This implies that the enriched and depleted end-members were likely generated at different melting degree. Such new information combined with the melt inclusion data (Starkey et al., 2012) and petrological evidence (e.g., Francis, 1985; Herzberg and O'Hara, 2002; Kent et al., 2004) suggests that both the mantle source and degree of partial melting for the enriched- and depleted-type of picrites are different.

Fig. 4. (**a**–**c)**: Correlations of selected refractory lithophile element ratios with Sm/Nd. A chondritic BSE (McDonough and Sun, 1995), average compositions of normal-MORB (N-MROB), ocean island basalt (OIB) (Sun and McDonough, 1989), depleted MORB mantle (DMM) (Workman and Hart, 2005) the range of early depleted reservoirs (EDR, black rectangles in **a** and **c**) (Carlson and Boyet, 2008), nonmodal batch partial melting (solid lines with cross), binary mixing (green dashed lines), super-chondritic Earth model (light pink colour area) and chondritic BSE (Caro and Bourdon, 2010) are shown. EMI and DMI represent the enriched and depleted types of melt inclusions from high $^{3}He/^{4}He$ BIWG picrites (Starkey et al., 2012). Numbers in italic mark partial melt fractions (%). (**d**–**f)**: Evolution of Nd-Sr-Hf-Os isotopes in the oldest mantle reservoir. The grey fields represent the isotopic evolution of the enriched end-member with Nb/La = 1.3–1.5 that originated from a chondritic BSE (McDonough and Sun, 1995). The $^{147}Sm/^{144}Nd$ ratios for both the enriched and

depleted end-members are estimated according to end-member Sm/Nd ratios. The Rb-Sr and Re-Os system for the enriched end-member is calculated using $(^{87}Rb/^{86}Sr)_E = K_E(^{87}Rb/^{86}Sr)_{CN}$ and $(^{187}Re/^{188}Os)_E = K_E(^{187}Re/^{188}Os)_{CN,}$ where $K_E = [(Nb/La)_E/(Nb/La)_{CN} + (Sm/Nd)_E/(Sm/Nd)_{CN}]/2$, with subscripts E and CN refer to the enriched end-member and the chondritic BSE, respectively. The same functions are used for calculating the isotopic systems of the depleted end-member. All isotopic evolution paths start at 4.4 Ga. The data sources for the BIWG picrites are the same as in Fig. 1. The nonmodal bacth melting was conducted at the garnet stability field accodring to $C_L = C_0/[D_0+F(1-P)]$, where D_0 is the initial bulk distirbution coefficient, and P is the bulk distribution coefficient determed by the melting model. F is the weight fraction of melt formed. C_0 and C_L are the concentrations of an element in the source and melt, respectively. The mineral/mlet parition coefficent datasets for olivine, clionpyroxenen, and orthophyroxenne are from (Kelemen et al., 2004), and the garnet/melt partition coeffiicent datasets are from (van Westrenen et al., 2000). The mineral model and melt reaction are from (Salters and Stracke, 2004).

Fig. 5. **(a)**: CI chondrite normalized (McDonough and Sun, 1995) trace-element-source budget of the early-formed silicate Earth. The nonchondritic BSE composition is based on the collision erosion model (O'Neill and Palme, 2008). The depleted mantle-1 and -2 were derived from the above nonchondritic BSE by respective extraction of 0.002 and 0.01 of basaltic melts to form protocrust, based on

317 mantle-crust partition coefficients (Workman and Hart, 2005) and the method
318 proposed by (Hofmann, 1988). The depleted end-member source is produced by 22%
319 partial melt of a depleted mantle-1 at 300-410 km. The enriched end-member source
320 is melt segregation from a basal magma ocean at ≥1,800 km (see text). The
321 back-calculated BIWG source (Jackson et al., 2010), estimates 1 and 2 for EDR
322 (Carlson and Boyet, 2008), enriched and depleted MORB mantles (Workman and
323 Hart, 2005), and chondritic BSE (McDonough and Sun, 1995) are also shown. **(b)**:
324 Evolution of $^{3}He/^{4}He$ in the Earth's silicate reservoirs. Evolution of $^{3}He/^{4}He$ for the
325 early formed dense chemical layer (blue colour area) is based on the method of (Class
326 and Goldstein, 2005) with the following constraints: (1) an initial $^{3}He/^{4}He$ =120 R_A;
327 (2) [^{3}He] ranging from 2.0 × 10^{11} atomsg^{-1} [25% higher than the estimate for
328 undegassed primitive mantle; Class and Goldstein, 2005) to 0.8 × 10^{10} atomsg^{-1} (10%
329 of the modern OIB source; Class and Goldstein, 2005) due to extraction of protocrust];
330 (3) U = 0.038 to 0.0028 ppm; Th = 0.0735 to 0.010 ppm. Evolution of deep mantle
331 (thick red line) and shallow mantle (grey band) are devolved from Lee et al (Lee et al.,
332 2010). The $^{3}He/^{4}He$ lower than 37R_A (open circles) were likely affected by
333 post-eruption ^{4}He accumulation and concomitant reduction of $^{3}He/^{4}He$ (Appendix Fig.
334 R4).

335 Fig. 6. (**a)**: Freezing of a magma ocean with nonchondritic BSE composition (Fig. 5a)
336 would have produced enriched dense melts below 1,800 km depth that accumulated at
337 the CMB, and 60% depletion of the BSE occurred at above 1,800 km depths due to
338 positive buoyance of the residual melt (e.g., Nomura et al., 2011). Shortly after

magma ocean crystallization, hot and deep melting of the upper mantle could have generated depleted dense melts at 410–300 km depth (e.g., Lee et al., 2010). The two types of dense liquids sunk and accumulated at the CMB to form a dense chemical layer. **(b)**: Late Archean to present-day mantle: melting is restricted to shallow depths. The dense chemical layer is likely hosted by large low-shear-wave velocity provinces (LLSVPs) and ultralow-velocity zones (ULVZs) (e.g., Nomura et al., 2011) and appears to have persisted for much of Earth's history unless pushed by deep-subducted slabs to rise up.

348 REFERENCES CITED

349 Allègre, C.J., 1982. Chemical geodynamics. Tectonophysics 81, 109-132.

350 Andrault, D., Petitgirard, S., Lo Nigro, G., Devidal, J.-L., Veronesi, G., Garbarino, G.,
351 Mezouar, M., 2012. Solid-liquid iron partitioning in Earth's deep mantle. Nature
352 487, 354-357.

353 Andreasen, R., Sharma, M., Subbarao, K.V., Viladkar, S.G., 2008. Where on Earth is
354 the enriched Hadean reservoir? Earth Planet. Sci. Lett. 266, 14-28.

355 Bennett, V.C., Brandon, A.D., Nutman, A.P., 2007. Coupled ^{142}Nd-^{143}Nd Isotopic
356 Evidence for Hadean Mantle Dynamics. Science 318, 1907-1910.

357 Campbell, I.H., O'Neill, S.C.H., 2012. Evidence against a chondritic Earth. Nature
358 483, 553-558.

359 Carlson, R.W., Boyet, M., 2008. Composition of the Earth's interior: the importance
360 of early events. Phil. Trans. R. Soc. A 366, 4077-4103.

361 Caro, G., 2011. Early Silicate Earth Differentiation. Annu. Rev. Earth Planet. Sci. 39,
362 31-58.

363 Caro, G., Bourdon, B., 2010. Non-chondritic Sm/Nd ratio in the terrestrial planets:
364 Consequences for the geochemical evolution of the mantle-crust system. Geochim.
365 Cosmochim. Acta 74, 3333-3349.

366 Caro, G., Bourdon, B., Halliday, A.N., Quitte, G., 2008. Super-chondritic Sm/Nd
367 ratios in Mars, the Earth and the Moon. Nature 452, 336-339.

368 Caro, G., Bourdon, B., Wood, B.J., Corgne, A., 2005. Trace-element fractionation in
369 Hadean mantle generated by melt segregation from a magma ocean. Nature 436,
370 246-249.

371 Class, C., Goldstein, S.L., 2005. Evolution of helium isotopes in the Earth's mantle.
372 Nature 436, 1107-1112.
373 Corgne, A., Liebske, C., Wood, B.J., Rubie, D.C., Frost, D.J., 2005. Silicate
374 perovskite-melt partitioning of trace elements and geochemical signature of a deep
375 perovskitic reservoir. Geochim. Cosmochim. Acta 69, 485-496.
376 Dale, C.W., Pearson, D.G., Starkey, N.A., Stuart, F.M., Ellam, R.M., Larsen, L.M.,
377 Fitton, J.G., Macpherson, C.G., 2009. Osmium isotopes in Baffin Island and West
378 Greenland picrites: Implications for the $^{187}Os/^{188}Os$ composition of the convecting
379 mantle and the nature of high $^{3}He/^{4}He$ mantle. Earth Planet. Sci. Lett. 278,
380 267-277.
381 de Leeuw, G.A.M., Carlson, R.W., Ellam, R.M., Stuart, F.M., 2010. Baffin Island
382 picrites contain normal terrestrial Nd-142/Nd-144: Implications for the source of
383 high He-3/He-4 in deep Earth. Geochim. Cosmochim. Acta 74, A219-A219.
384 Francis, D., 1985. The Baffin Bay lavas and the value of picrites as analogues of
385 primary magmas. Contrib. Mineral. Petrol. 89, 144-154.
386 Heber, V.S., Brooker, R.A., Kelley, S.P., Wood, B.J., 2007. Crystal–melt partitioning
387 of noble gases (helium, neon, argon, krypton, and xenon) for olivine and
388 clinopyroxene. Geochim. Cosmochim. Acta 71, 1041-1061.
389 Herzberg, C., O'Hara, M.J., 2002. Plume-associated Ultramafic magmas of
390 Phanerozoic age. J. Paleontol. 43, 1857-1883.
391 Hofmann, A.W., 1988. Chemical differentiation of the Earth: the relationship between
392 mantle, continental crust, and oceanic crust. Earth Planet. Sci. Lett. 90, 297-314.

393 Hofmann, A.W., 1997. Mantle geochemistry: the message from oceanic volcanism.
394 Nature 385, 219-229.
395 Jackson, M.G., Carlson, R.W., 2011. An ancient recipe for flood-basalt genesis.
396 Nature 476, 316-319.
397 Jackson, M.G., Carlson, R.W., Kurz, M.D., Kempton, P.D., Francis, D., Blusztajn, J.,
398 2010. Evidence for the survival of the oldest terrestrial mantle reservoir. Nature
399 466, 853-856.
400 Kelemen, P.B., Yogodzinski, G.M., Scholl, D.W., 2004. Alongstrike variation in lavas
401 of the Aleutian island arc: implications for the genesis of high Mg# andesite and
402 the continental crust,. AGU Monograph.
403 Kent, A.J.R., Stolper, E.M., Francis, D., Woodhead, J., Frei, R., Eiler, J., 2004. Mantle
404 heterogeneity during the formation of the North Atlantic Igneous Province:
405 Constraints from trace element and Sr-Nd-Os-O isotope systematics of Baffin
406 Island picrites. Geochem. Geophys. Geosyst. 5, Q11004.
407 Labrosse, S., Hernlund, J.W., Coltice, N., 2007. A crystallizing dense magma ocean at
408 the base of the Earth's mantle. Nature 450, 866-869.
409 Larsen, L.M., Pedersen, A.K., 2009. Petrology of the Paleocene Picrites and Flood
410 Basalts on Disko and Nuussuaq, West Greenland. J. Petrol. 50, 1667-1711.
411 Lee, C.-T.A., Luffi, P., Hoink, T., Li, J., Dasgupta, R., Hernlund, J., 2010.
412 Upside-down differentiation and generation of a 'primordial' lower mantle. Nature
413 463, 930-933.
414 Li, Z.-X., Zhong, S., 2009. Supercontinent-superplume coupling, true polar wander

415 and plume mobility: Plate dominance in whole-mantle tectonics. Phys. Earth
416 Planet Interiors 176, 143-156.
417 Lightfoot, P.C., Hawkesworth, C.J., Olshefsky, K., Green, T., Doherty, W., Keays,
418 R.R., 1997. Geochemistry of Tertiary tholeiites and picrites from Qeqertarssuaq
419 (Disko Island) and Nuussuaq, West Greenland with implications for the mineral
420 potential of comagmatic intrusions. Contrib. Mineral. Petrol. 128, 139-163.
421 McDonough, W.F., Sun, S.s., 1995. The composition of the Earth. Chem. Geol. 120,
422 223-253.
423 Miller, G.H., Stolper, E.M., Ahrens, T.J., 1991. The equation of state of a molten
424 komatiite. 2. Application to komatiite petrogenesis and the Hadean mantle. J.
425 Geophys. Res. 96, 11849-11864.
426 Moynier, F., Yin, Q.-Z., Irisawa, K., Boyet, M., Jacobsen, B., Rosing, M.T., 2010.
427 Coupled ^{182}W-^{142}Nd constraint for early Earth differentiation. PNAS 107,
428 10810-10814.
429 Nomura, R., Ozawa, H., Tateno, S., Hirose, K., Hernlund, J., Muto, S., Ishii, H.,
430 Hiraoka, N., 2011. Spin crossover and iron-rich silicate melt in the Earth's deep
431 mantle. Nature 473, 199-202.
432 O'Neill, H.S.C., Palme, H., 2008. Collisional Erosion and the Non-Chondritic
433 Composition of the Terrestrial Planets. Phil. Trans. R. Soc. A 366, 4205-4238.
434 Paul, D., White, W.M., Turcotte, D.L., 2002. Modelling the isotopic evolution of the
435 Earth. Phil. Trans. R. Soc. Lond. A 360, 2433-2474.
436 Putirka, K.D., Perfit, M., Ryerson, F.J., Jackson, M.G., 2007. Ambient and excess

437 mantle temperatures, olivine thermometry, and active vs. passive upwelling. Chem.
438 Geol. 241, 177-206.
439 Robillard, I., Francis, D., Ludden, J.N., 1992. The relationship between E- and N-type
440 magmas in the Baffin Bay Lavas. Contrib. Mineral. Petrol. 112, 230-241.
441 Salters, V.J.M., Stracke, A., 2004. Composition of the depleted mantle. Geochem.
442 Geophys. Geosyst. 5, Q05B07.
443 Schaefer, B.F., Parkinson, I.J., Hawkesworth, C.J., 2000. Deep mantle plume osmium
444 isotope signature from West Greenland Tertiary picrites. Earth Planet. Sci. Lett.
445 175, 105-118.
446 Starkey, N., Stuart, F., Ellam, R., Fitton, J., Basu, S., Larsen, L., 2009. Helium
447 isotopes in early Iceland plume picrites: Constraints on the composition of high
448 $^{3}He/^{4}He$ mantle. Earth Planet. Sci. Lett. 277, 91-100.
449 Starkey, N.A., Fitton, J.G., Stuart, F.M., Larsen, L.M., 2012. Melt inclusions in
450 olivines from early Iceland plume picrites support high $^{3}He/^{4}He$ in both enriched
451 and depleted mantle. Chem. Geol. 306–307, 54-62.
452 Steinberger, B., Torsvik, T.H., 2012. A geodynamic model of plumes from the margins
453 of Large Low Shear Velocity Provinces. Geochem. Geophys. Geosyst. 13,
454 Q01W09.
455 Stolper, E., Walker, D., Hager, B.H., Hays, J.F., 1981. Melt segregation from partially
456 molten source regions: the importance of melt density and source region size. J.
457 Geophys. Res. 86, 6261-6271.
458 Sun, S.-s., McDonough, W.F., 1989. Chemical and isotopic systematics of oceanic

459 basalts: implications for mantle composition and processes., in: Saunders, A.D.,
460 Norry, M.J. (Eds.), Magmatism in the Ocean Basins. Geol. Soc. London, Spec.
461 Publ., pp. 313-345.
462 Suzuki, A., Ohtani, E., Kato, T., 1998. Density and thermal expansion of a peridotite
463 melt at high pressure. Phys. Earth Planet. Inter. 107, 53-61.
464 van Westrenen, W., Blundy, J.D., Wood, B.J., 2000. Effect of Fe (super 2+) on
465 garnet-melt trace element partitioning: experiments in FCMAS and quantification
466 of crystal-chemical controls in natural systems. Lithos 53, 189-201.
467 Wang, X.-C., Li, Z.-X., Li, X.-H., Li, J., Liu, Y., Long, W.-G., Zhou, J.-B., Wang, F.,
468 2012. Temperature, Pressure, and Composition of the Mantle Source Region of
469 Late Cenozoic Basalts in Hainan Island, SE Asia: a Consequence of a Young
470 Thermal Mantle Plume close to Subduction Zones? J. Petrol. 53, 177-233.
471 Workman, R.K., Hart, S.R., 2005. Major and trace element composition of the
472 depleted MORB mantle (DMM). Earth Planet. Sci. Lett. 231, 53-72.
473 Zindler, A., Hart, S., 1986. Chemical geodynamics. Annu. Rev. Earth Planet. Sci. 14,
474 493-571.
475

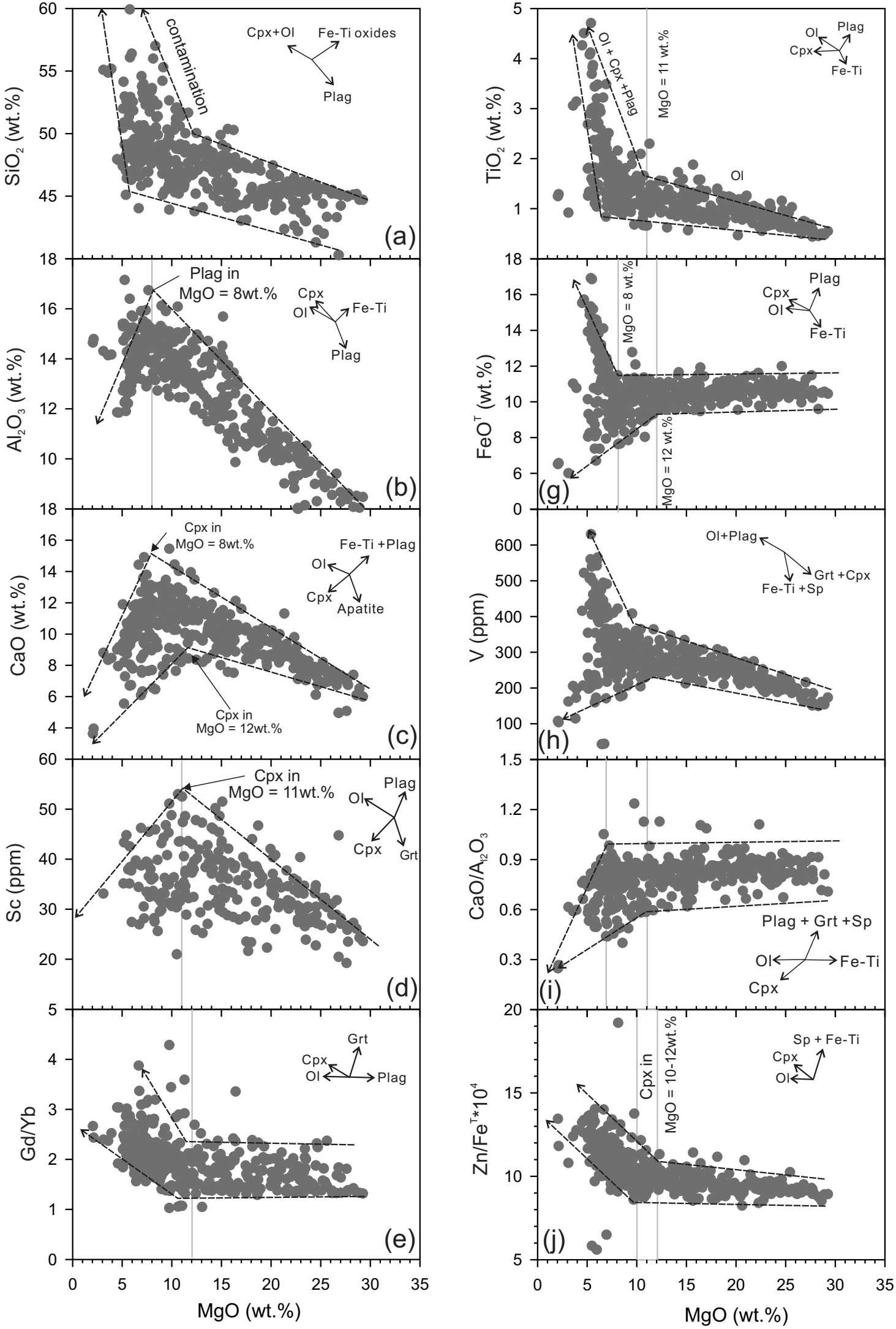
SiO2 (wt.%)
contamination
Cpx+Ol
Fe-Ti oxides
Plag
(a)
Al2O3 (wt.%)
Plag in
MgO = 8wt.%
Cpx
Ol
Fe-Ti
Plag
(b)
CaO (wt.%)
Cpx in
MgO = 8wt.%
Fe-Ti +Plag
Ol
Cpx
Apatite
Cpx in
MgO = 12wt.%
(c)
Sc (ppm)
Cpx in
MgO = 11wt.%
Plag
Ol
Cpx
Grt
(d)
Gd/Yb
Grt
Cpx
Ol
Plag
(e)
MgO (wt.%)
TiO2 (wt.%)
Ol + Cpx +Plag
MgO = 11 wt.%
Ol
Plag
Cpx
Fe-Ti
FeOT (wt.%)
MgO = 8 wt.%
MgO = 12 wt.%
Plag
Cpx
Ol
Fe-Ti
(g)
V (ppm)
Ol+Plag
Grt +Cpx
Fe-Ti +Sp
(h)
CaO/Al2O3
Plag + Grt +Sp
Ol
Fe-Ti
Cpx
(i)
Zn/FeT*10^4
Cpx in
MgO = 10-12wt.%
Sp + Fe-Ti
Cpx
Ol
(j)
MgO (wt.%)

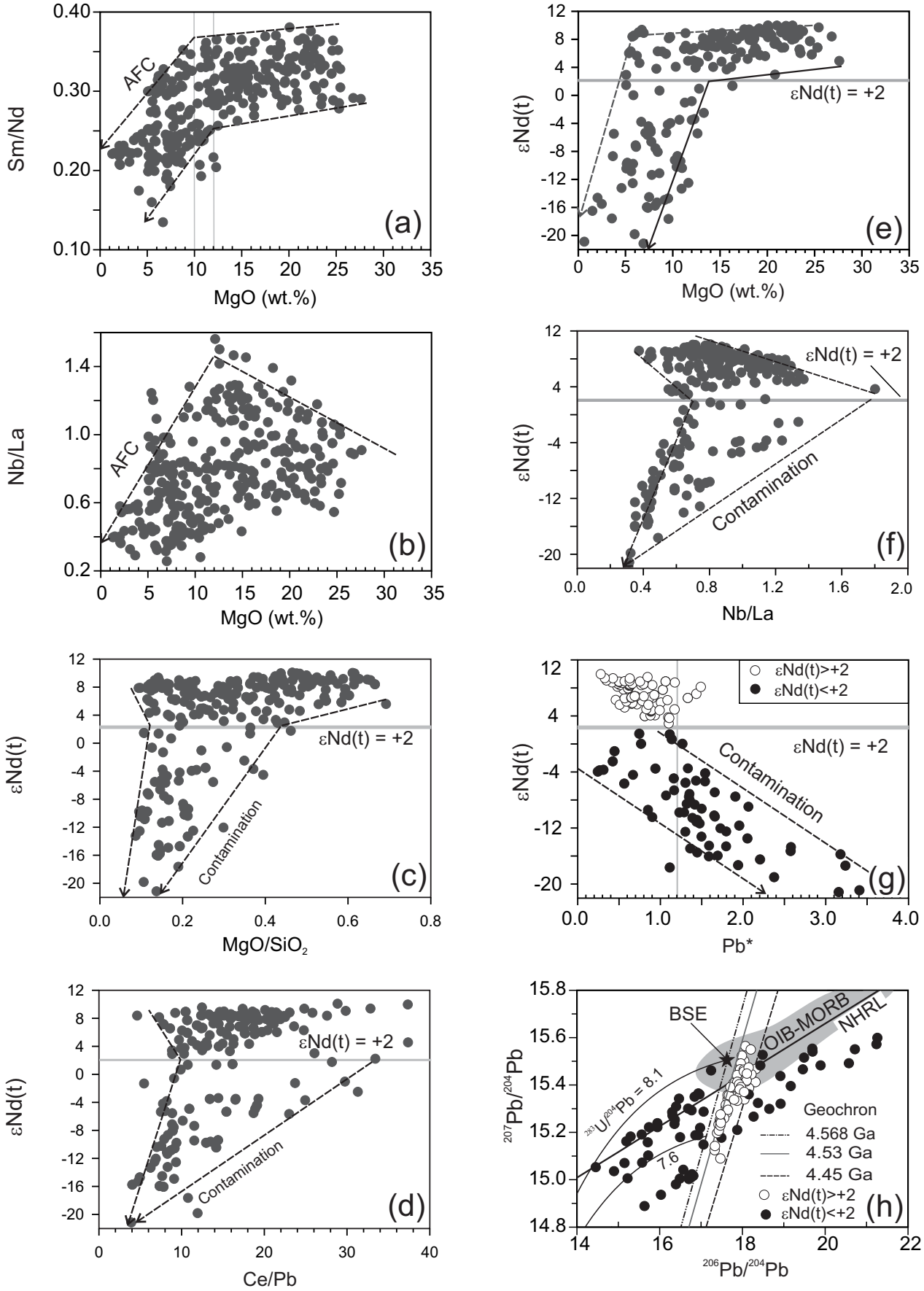
(a)
Sm/Nd
MgO (wt.%)
AFC
(b)
Nb/La
MgO (wt.%)
AFC
(c)
εNd(t)
MgO/SiO2
εNd(t) = +2
Contamination
(d)
εNd(t)
Ce/Pb
εNd(t) = +2
Contamination
(e)
εNd(t)
MgO (wt.%)
εNd(t) = +2
(f)
εNd(t)
Nb/La
εNd(t) = +2
Contamination
(g)
εNd(t)
Pb*
εNd(t)>+2
εNd(t)<+2
εNd(t) = +2
Contamination
(h)
207Pb/204Pb
206Pb/204Pb
BSE
OIB-MORB
NHRL
238U/204Pb = 8.1
7.6
Geochron
4.568 Ga
4.53 Ga
4.45 Ga
εNd(t)>+2
εNd(t)<+2

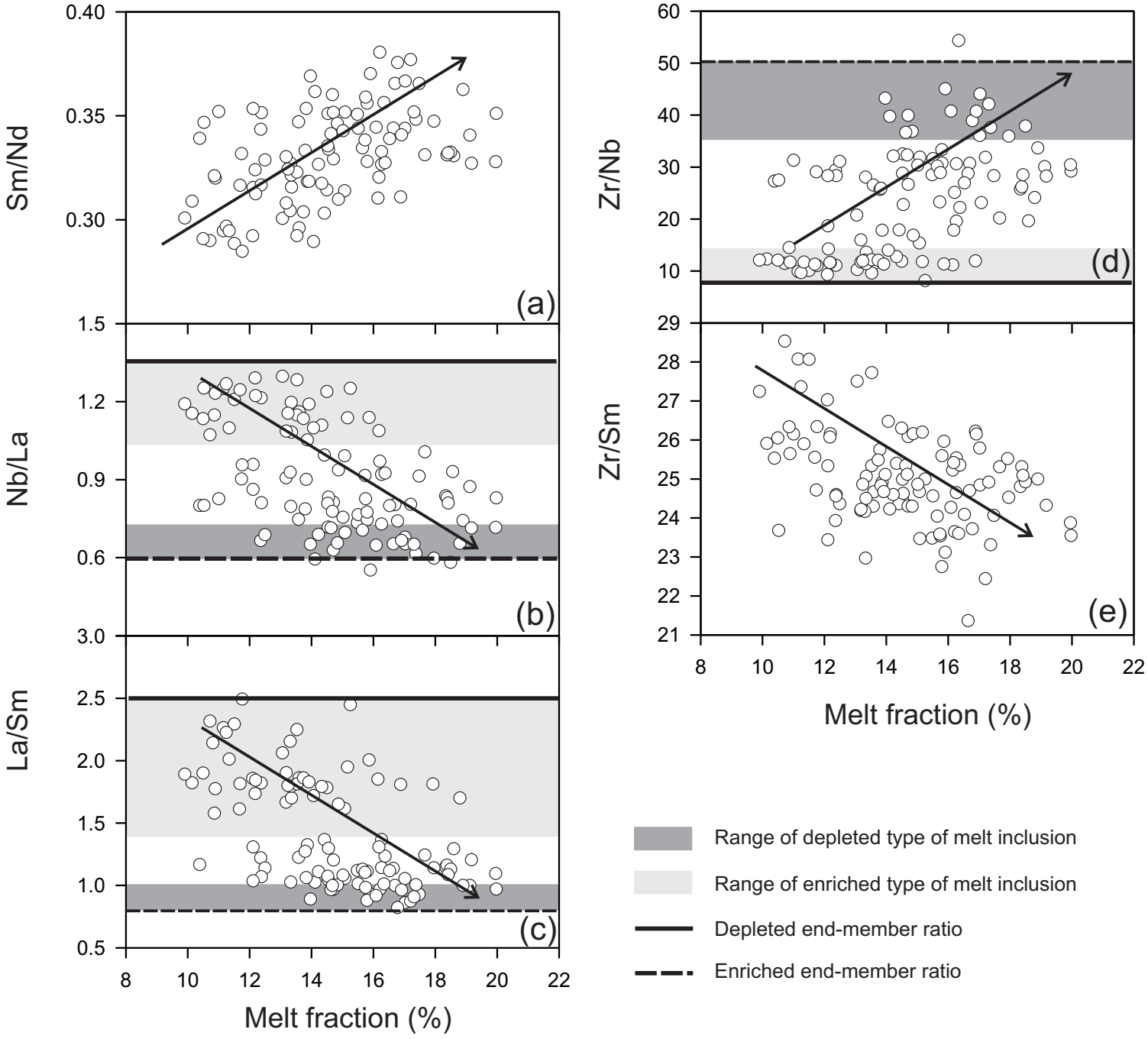
Sm/Nd
0.40
0.35
0.30
1.5
(a)
Nb/La
1.2
0.9
0.6
3.0
(b)
La/Sm
2.5
2.0
1.5
1.0
0.5
(c)
8
10
12
14
16
18
20
22
Melt fraction (%)
Zr/Nb
60
50
40
30
20
10
(d)
Zr/Sm
29
28
27
26
25
24
23
22
21
(e)
Melt fraction (%)
Range of depleted type of melt inclusion
Range of enriched type of melt inclusion
Depleted end-member ratio
Enriched end-member ratio

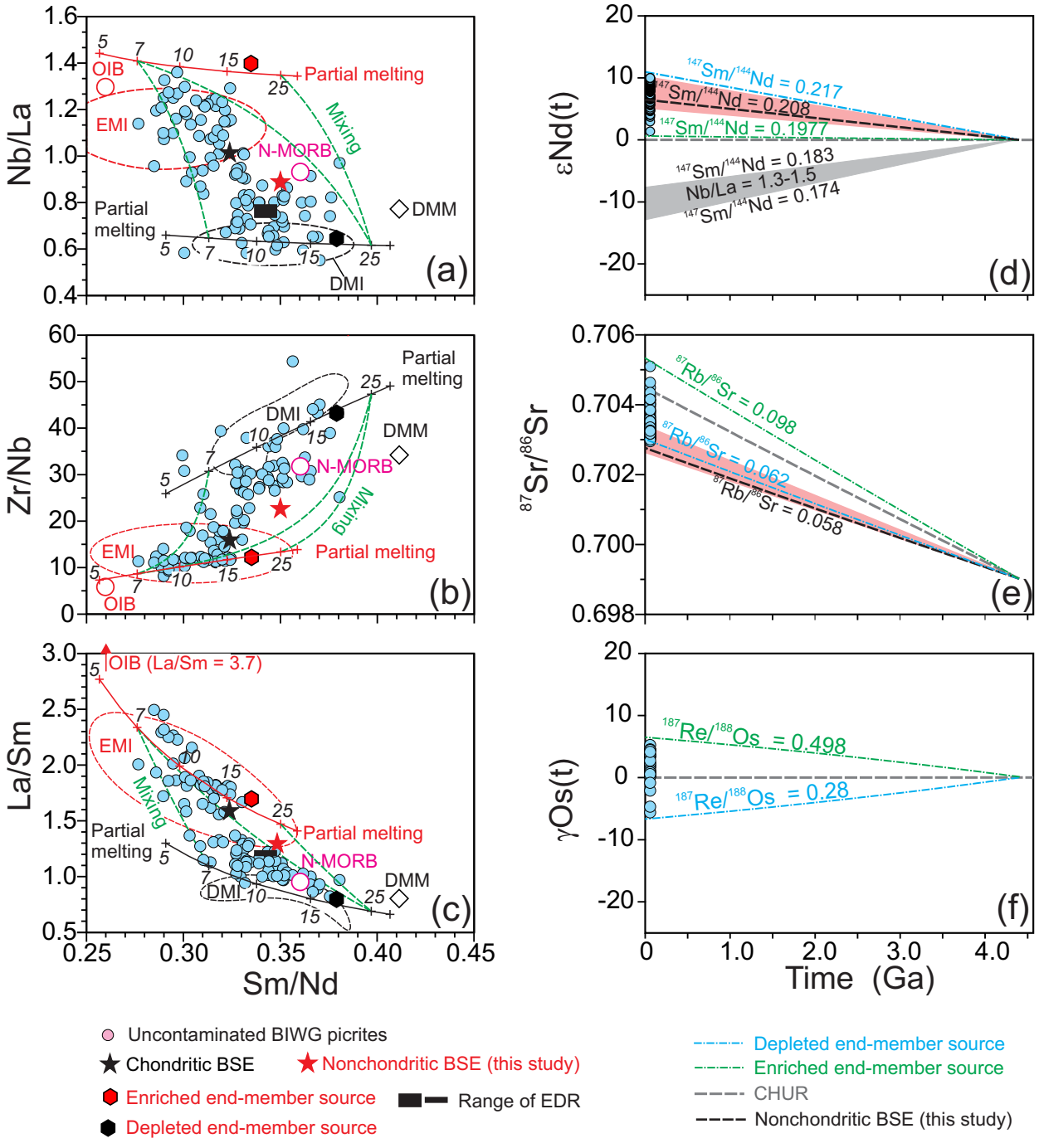
Nb/La
Zr/Nb
La/Sm
Sm/Nd
εNd(t)
87Sr/86Sr
γOs(t)
Time (Ga)
OIB
EMI
N-MORB
Partial melting
DMM
DMI
Mixing
(a)
(b)
(c)
(d)
(e)
(f)
147Sm/144Nd = 0.217
147Sm/144Nd = 0.208
147Sm/144Nd = 0.1977
147Sm/144Nd = 0.183
Nb/La = 1.3-1.5
147Sm/144Nd = 0.174
87Rb/86Sr = 0.098
87Rb/86Sr = 0.062
87Rb/86Sr = 0.058
187Re/188Os = 0.498
187Re/188Os = 0.28
OIB (La/Sm = 3.7)
Uncontaminated BIWG picrites
Chondritic BSE
Nonchondritic BSE (this study)
Enriched end-member source
Depleted end-member source
Range of EDR
Depleted end-member source
Enriched end-member source
CHUR
Nonchondritic BSE (this study)

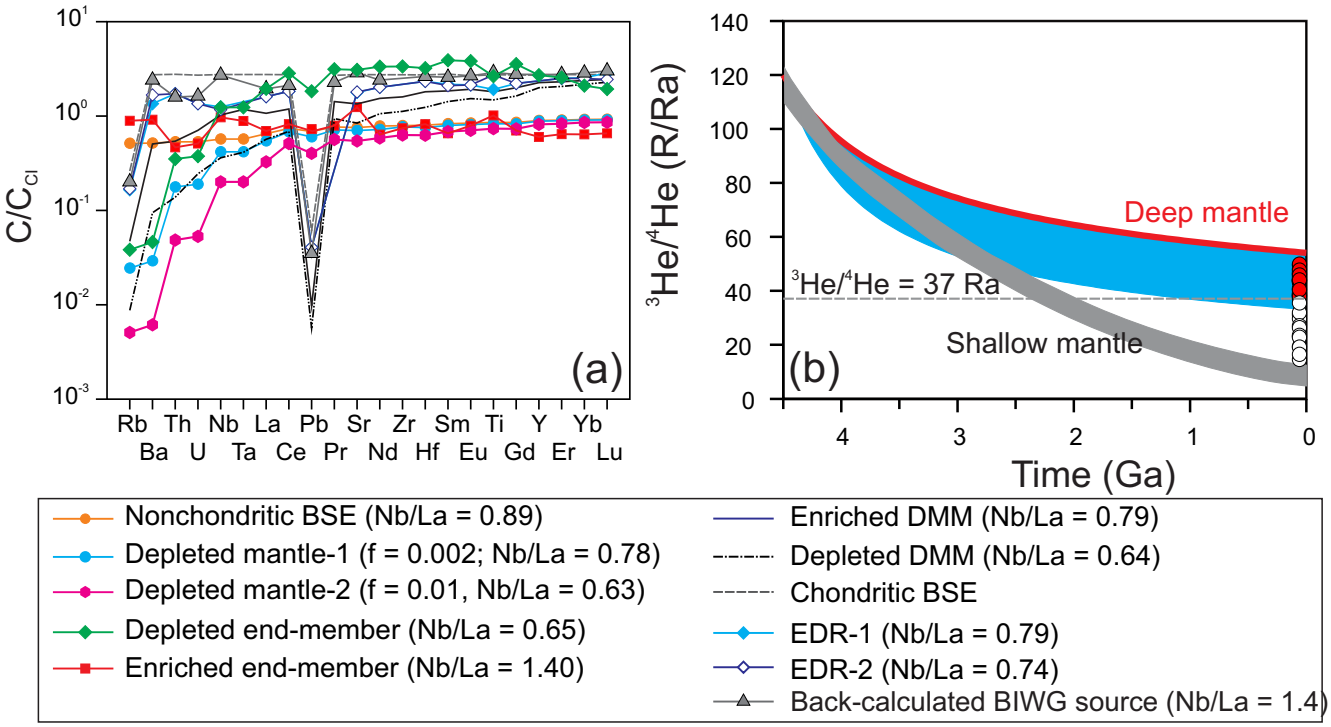
C/C_CI
10^1
10^0
10^-1
10^-2
10^-3
Rb Th Nb La Pb Sr Zr Sm Ti Y Yb
Ba U Ta Ce Pr Nd Hf Eu Gd Er Lu
(a)
3He/4He (R/Ra)
140
120
100
80
60
40
20
0
Deep mantle
3He/4He = 37 Ra
Shallow mantle
(b)
4
3
2
1
0
Time (Ga)
Nonchondritic BSE (Nb/La = 0.89)
Depleted mantle-1 (f = 0.002; Nb/La = 0.78)
Depleted mantle-2 (f = 0.01, Nb/La = 0.63)
Depleted end-member (Nb/La = 0.65)
Enriched end-member (Nb/La = 1.40)
Enriched DMM (Nb/La = 0.79)
Depleted DMM (Nb/La = 0.64)
Chondritic BSE
EDR-1 (Nb/La = 0.79)
EDR-2 (Nb/La = 0.74)
Back-calculated BIWG source (Nb/La = 1.4)

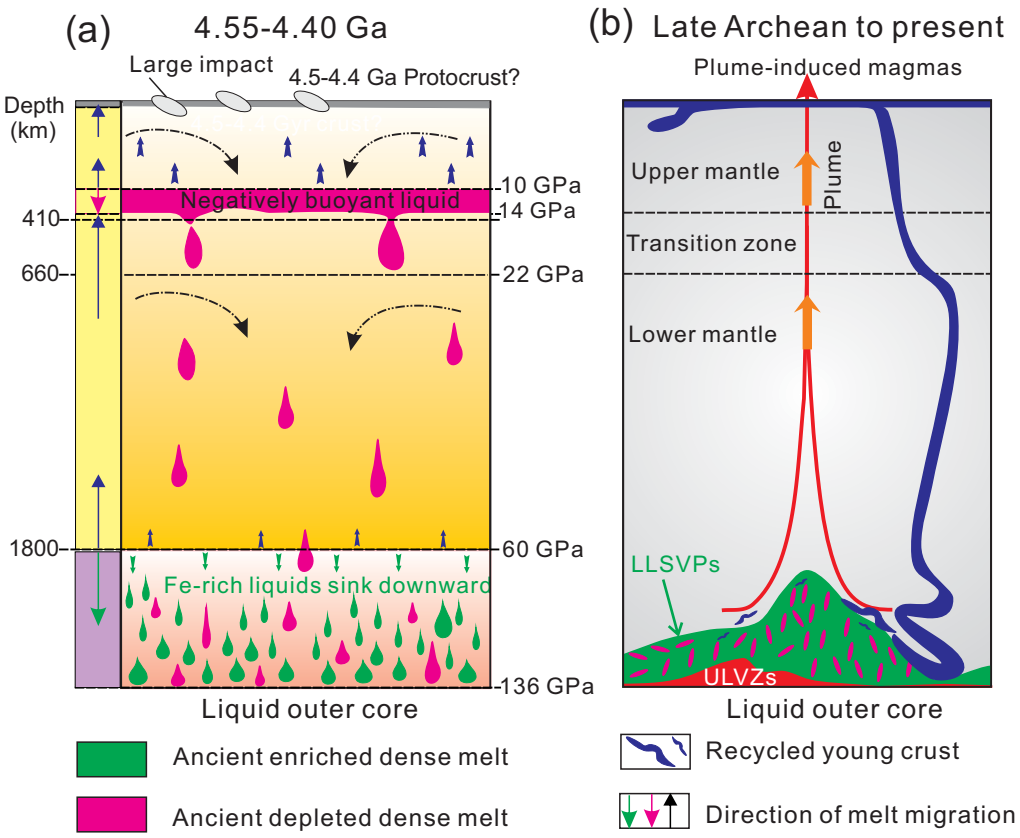
(a)
4.55-4.40 Ga
Large impact
4.5-4.4 Ga Protocrust?
Depth (km)
Negatively buoyant liquid
10 GPa
14 GPa
410
660
22 GPa
1800
60 GPa
Fe-rich liquids sink downward
136 GPa
Liquid outer core
Ancient enriched dense melt
Ancient depleted dense melt
(b)
Late Archean to present
Plume-induced magmas
Upper mantle
Plume
Transition zone
Lower mantle
LLSVPs
ULVZs
Liquid outer core
Recycled young crust
Direction of melt migration